



Evaluation of pelvic structural abnormalities in primiparous women with stress urinary incontinence

Li Shi¹ · Yujiao Zhao² · Weijun Li¹ · Lihua Chen² · Wen Shen² · Lidong Zhai¹

Received: 11 July 2023 / Accepted: 8 October 2023 / Published online: 15 November 2023
© The International Urogynecological Association 2023

Abstract

Introduction and hypothesis The objective was to evaluate the morphological characteristics of pelvic floor structure specific to de novo stress urinary incontinence (SUI) in primiparous women using three-dimensional (3D) reconstruction fusion technology based on static MRI combined with dynamic MRI.

Methods Eighty-one primiparous women after the first vaginal delivery were studied, 40 with SUI and 41 without SUI. 3D reconstruction models based on static MRI were used to describe the anatomical abnormalities of pelvic floor tissues. Dynamic MRI was used to describe segmental activities of the urethra and vagina. The relationship between the morphometry and postpartum SUI was evaluated by logistic regression analysis and receiver operator characteristic curve.

Results The differences in the distance from the bladder neck to the pubic symphysis (BSD), the angle between the posterior wall of the urethra and the anterior wall of the vagina, the width of the distal region of the vagina, urethral length, urethral compression muscle volume (CUV), and pubovisceral muscle volume, puborectal muscle volume, were measured, and except for the extremity of the anterior urethral wall, the total displacements (TDs) of the other sites between the two groups were statistically significant ($p < 0.05$). Logistic regression analysis showed that the BSD decreased, the CUV decreased, the TDs of the first site and the eighth site increment correlated significantly with postpartum SUI occurrence ($p < 0.05$).

Conclusions 3D reconstruction fusion technology provides an important support for a precise assessment of the pelvic floor dysfunction. The BSD, CUV, and iliococcygeus muscle volume have certain values in predicting de novo SUI after first vaginal birth.

Keywords Stress urinary incontinence · Primiparous women · Three-dimensional reconstruction · Dynamic magnetic resonance imaging · Urethral and vaginal mobility

Li Shi and Yujiao Zhao contributed equally to this work.

✉ Wen Shen
shenwen66happy@126.com

✉ Lidong Zhai
zhailidong2005@126.com

¹ Department of Anatomy and Histology, School of Basic Medical Sciences, Tianjin Medical University, Tianjin 300070, China

² Department of Radiology, Tianjin First Central Hospital, School of Medicine, Nankai University, Fukang Road No. 24, Nankai District, Tianjin 300192, China

Introduction

Stress urinary incontinence (SUI) is defined as the involuntary outflow of urine when abdominal pressure increases [1] and is the most common pelvic floor dysfunction disease. Delivery is one of the main risk factors for the development of SUI in women [2]. De novo SUI is defined as a condition in which the primiparous woman is normal before delivery and experiences SUI symptoms after delivery.

Although postpartum symptoms in women change over time, the pathogenesis of de novo SUI has also received continuous attention. The parameters related to de novo SUI, such as urethral length (UL), bladder neck mobility, and levator ani muscle (LAM) morphology, have been measured on two-dimensional (2D) planes to identify impairments specific to SUI [3, 4]. However, measuring UL as a straight line has limitations [4–6], as the shape of the deformed

urethra is irregular. It is also difficult to measure the volume and surface area of an irregular structure in a 2D plane. The UL, thickness and volume of LAM can be analyzed and measured directly by three-dimensional (3D) reconstruction. It is widely recognized as a useful tool for evaluating various functional disorders owing to its accuracy, visualization, and multi-angle observation [7, 8], which compensates for the shortcomings of 2D measurements. To our knowledge, 3D reconstructions have not been previously used to perform various measurements and analyses of different parts of the vagina.

In recent years, studies have shown that hyperactivity of the middle urethra is a risk factor for SUI [9]. In the study of segmental activities of the urethra, the urethra has been considered to be a whole division [10, 11], but the movement patterns and segmental activities of the anterior and posterior walls of the urethra, as well as the anterior and posterior walls of the vagina alone, have received little attention.

The main aims of the study are as follows: first, to describe the anatomical abnormalities of the routine parameters of pelvic floor structures, and the abnormalities of the volume, thickness, and the three diameter lines of the proximal and distal vaginal areas of de novo SUI after the first vaginal delivery, in which 3D reconstruction fusion models are used based on a static MRI; second, to determine the differences in motion patterns and segmental activities of the anterior and posterior walls of the urethra and the vagina between the SUI group and the normal group based on a dynamic MRI; finally, to analyze the predictive values of these parameters for the occurrence of de novo SUI after the first vaginal delivery.

Materials and methods

Patients

In this retrospective cross-sectional study, MR images of 91 primiparous women delivered via vaginal delivery who underwent postpartum pelvic floor reexamination in Tianjin First Central Hospital from October 2015 to December 2017 were collected. The participants included 43 primiparous women diagnosed with SUI through the urinary incontinence questionnaire score, who reported normal prenatal conditions and 48 healthy primiparous women who were matched in age and body mass index and did not show any abnormalities through medical history, clinical examination, questionnaire survey, and imaging examination. Before the examination, the patients were instructed to assume a supine position with a wedge-shaped cushion placed under the knee to simulate the lithotomy position to maintain consistency in the pelvic position, thereby standardizing the slice angle, and patients were trained to perform the resting-force

movement (Valsalva). After subjects had undergone a 2-h period of urine holding to maintain a moderate bladder filling, static and dynamic scan examinations were performed using a Philips Ingenia 3.0 T magnetic resonance scanner and a 16-channel phased array body coil. The MRI examination conducted in this study was a scientific research scanning protocol. Supplementary file1 shows specific scanning parameters. Inclusion criteria were:

1. Primiparas who gave birth through the vagina for about 6 weeks
2. In the SUI group, involuntary urine leakage occurred during a sudden increase in abdominal pressure (such as coughing, sneezing, laughing, or exercising) at least twice a week

Exclusion criteria were:

1. History of pelvic surgery
2. Incomplete clinical data, missing images and poor imaging quality
3. Postpartum pelvic organ prolapse was excluded in the SUI group

The study process conformed to the Declaration of Helsinki (as revised in 2013) and was approved by the Institutional Review Board of Tianjin First Central Hospital (registration ID2018NO22KY).

3D reconstruction and measurements

The collected T₂WI MRI was imported into Mimics 19.0 in DICOM format, and the 3D reconstruction of the lower urinary tract tissue was completed by specialized researchers. In order to achieve precise reconstruction of the lower urinary tract, this study applied corresponding 3D model-based registration for creation of the fusion 3D models. In the first step, three 3D models of the same structure were reconstructed based on the horizontal, coronal, and sagittal MRI. In the second step, based on the same coordinate system, the corresponding 3D models are accurately fitted in Geomagic Studio 14.0 software. For this method, each 3D structure achieved reconstruction and fusion, which made the models more realistic and favorable for measurement analysis. And then, we measured the 3D models with 3-matic 11.0.

The steps for the measurements of the proximal and the distal regions of the vagina were as follows. In the first step, a horizontal plane was identified using 3-matic software according to a point that was used to mark the lowest point of the bladder neck in a 2D plane. In the second step, the vagina was cut into two parts above and below the bladder neck based on the determined plane using the "plane cutting"

Table 1 Comparison of 3D measurement parameters between the two groups (mean ± SD)

| Parameters | SUI | Non-SUI | <i>p</i> |
|---|----------------|---------------|----------|
| BSD (mm) | 9.07 ± 5.04 | 15.00 ± 3.62 | 0.000* |
| LD-Angle (°) | 138.82 ± 5.11 | 138.59 ± 6.66 | 0.860 |
| RD-Angle (°) | 139.53 ± 5.97 | 139.71 ± 6.36 | 0.891 |
| LR-Angle (°) | 4.15 ± 3.55 | 3.53 ± 2.66 | 0.511 |
| Urethral volume (cm ³) | 3.05 ± 0.75 | 4.35 ± 6.97 | 0.172 |
| Urethral surface area (cm ²) | 1.54 ± 0.28 | 1.75 ± 1.46 | 0.996 |
| Urethral width (mm) | 19.56 ± 5.36 | 17.08 ± 4.07 | 0.016** |
| Anterior posterior diameter of the urethra (mm) | 17.98 ± 3.40 | 17.60 ± 3.38 | 0.493 |
| Urethral length (mm) | 26.72 ± 3.39 | 30.18 ± 3.12 | 0.000* |
| A-Angle (°) | 9.45 ± 7.12 | 8.87 ± 6.44 | 0.821 |
| B-Angle (°) | 164.62 ± 11.79 | 168.27 ± 9.57 | 0.162 |
| C-Angle (°) | 8.56 ± 5.90 | 5.72 ± 3.63 | 0.034** |
| The proximal region of the vagina volume (cm ³) | 19.35 ± 10.32 | 22.22 ± 12.98 | 0.273 |
| Anterior posterior diameter of the proximal region of the vagina (mm) | 35.52 ± 9.91 | 36.09 ± 10.11 | 0.798 |
| Width of the proximal region of the vagina (mm) | 75.50 ± 18.44 | 78.61 ± 19.61 | 0.247 |
| Length of the proximal region of the vagina (mm) | 20.17 ± 8.80 | 19.49 ± 9.79 | 0.981 |
| Distal region of the vagina volume (cm ³) | 13.91 ± 5.06 | 14.13 ± 3.49 | 0.824 |
| Anterior posterior diameter of the distal region of the vagina (mm) | 27.69 ± 4.93 | 28.42 ± 5.84 | 0.985 |
| Width of the distal region of the vagina (mm) | 47.81 ± 7.90 | 51.69 ± 7.58 | 0.026** |
| Length of the distal region of the vagina (mm) | 29.49 ± 5.716 | 28.52 ± 4.19 | 0.385 |
| Volume of the obturator internus muscles (cm ³) | 65.67 ± 14.65 | 66.97 ± 12.55 | 0.667 |
| Volume of the obturator internus muscles (cm ²) | 22.03 ± 3.29 | 22.61 ± 2.41 | 0.361 |
| Volume of the urethral cavity (cm ³) | 0.19 ± 0.08 | 0.17 ± 0.13 | 0.237 |
| Volume of the urethral cavity (cm ²) | 0.23 ± 0.09 | 0.21 ± 0.12 | 0.438 |
| Length of the urethral cavity (mm) | 15.97 ± 5.91 | 15.01 ± 7.09 | 0.891 |
| Anterior posterior diameter of the urethral cavity (mm) | 6.15 ± 1.95 | 6.57 ± 2.88 | 0.448 |
| Width of the urethral cavity (mm) | 6.13 ± 1.68 | 5.73 ± 2.56 | 0.199 |
| Width of the urethral cavity (cm ³) | 0.14 ± 0.10 | 0.29 ± 0.16 | 0.000* |
| Surface area of the compressor urethra (cm ²) | 0.41 ± 0.21 | 0.68 ± 0.28 | 0.000* |
| Surface area of the compressor urethra (mm) | 3.67 ± 1.53 | 4.97 ± 1.49 | 0.000* |
| Iliococcygeus muscle volume (cm ³) | 11.06 ± 3.69 | 8.35 ± 3.04 | 0.001*** |
| Iliococcygeus muscle volume (cm ²) | 12.00 ± 2.34 | 8.54 ± 1.91 | 0.000* |
| Iliococcygeus muscle volume (mm) | 5.53 ± 0.77 | 5.57 ± 0.99 | 0.847 |
| Pubovisceral muscle volume (cm ³) | 5.65 ± 1.39 | 6.67 ± 1.69 | 0.004*** |
| Surface area of the pubovisceral muscle (cm ²) | 6.48 ± 1.34 | 7.14 ± 1.33 | 0.030** |
| Thickness of the pubovisceral muscle (mm) | 6.83 ± 1.00 | 6.75 ± 0.94 | 0.667 |
| Thickness of the pubovisceral muscle (cm ³) | 6.51 ± 2.60 | 8.71 ± 1.64 | 0.000* |
| Thickness of the pubovisceral muscle (cm ²) | 6.15 ± 1.95 | 8.90 ± 1.46 | 0.000* |
| Thickness of the puborectal muscle (mm) | 6.44 ± 0.92 | 5.89 ± 0.78 | 0.003*** |

SD standard deviation, *BSD* distance from the bladder neck to the upper edge of the pubic symphysis; *LD-Angle* inclination angle between the base of the levator ani muscle and the lateral wall of the left part, *RD-Angle* inclination angle between the base of the levator ani muscle and the lateral wall of the right part, *LR-Angle* absolute value of the difference between the RD-Angle and the LD-Angle, *UA* anterior posterior diameter of the urethra, *A-Angle* the angle of the central line of the proximal urethra and the distal urethra, *B-Angle* the angle of the central line of the distal urethra and the distal urethra, *C-Angle* the angle between the posterior wall of the urethra and the anterior wall of the vagina

p* < 0.0001; *p* < 0.05; ****p* < 0.01

tool of 3-matic software. In this method, the different regions of the vagina achieved division.

The urethral compression muscle (CU) volume (CUV), the surface area of the CU (CUS), the iliococcygeus muscle

(IC) volume (ICV), the surface area of IC (ICS), the pubovisceral muscle (PVi) volume (PViV), the surface area of the PVi (PViS), the puborectal muscle (PR) volume (PRV), the surface area of PR (PRS), the urethral volume (UV),

the urethral surface area, the volume of the UC, the surface area of the UC, the vaginal surface area, the proximal region of the vagina volume, the distal region of the vagina volume, the volume of the obturator internus muscles, and the surface area of the obturator internus muscles were directly viewed by the 3-matic software.

The procedure for measuring diameter lines is as follows: first, the entities were analyzed by means of 3-matic software for extreme values on the X, Y, and Z axes, the leftmost and rightmost points were analyzed on the X axis, the highest and lowest points were analyzed on the Y axis, the anterior and final points were obtained on the Z axis, and next, the distance between the two poles value points on each axis were measured in a straight line. Finally, the urethral width (UW), the anterior and posterior diameter of the urethra, the width of the urethral cavity, the length of the urethral cavity, the anterior–posterior diameter of the urethral cavity, the width of the proximal region of the vagina, the length of the proximal region of the vagina (VPL), the anterior–posterior diameter of the proximal region of the vagina, the width of the distal region of the vagina (VDW), the length of the distal region of the vagina (VDL), and the anterior–posterior diameter of the distal region of the vagina achieve the measurement of the three diameter lines. The thickness measurements of the compressor urethra (CUT), the iliococcygeus muscle (ICT), the pubovisceral muscle (PViT), the puborectal muscle (PRT) were directly analyzed and realized by the 3-matic "wall thickness analysis" tool.

The angle between the lower and anterior lower edges of the right part and the left part of the LAM was defined as the RD-Angle and the LD-Angle respectively. LR-Angle was the absolute value of the difference between the RD-Angle and the LD-Angle. The center lines of the distal and proximal urethra and vagina were analyzed using the 3-matic software. The angles between the central line of the proximal and the distal urethra and the coronal plane were defined as the A-Angle and the B-Angle. The angle between the posterior wall of the urethra and the anterior wall of the vagina was defined as the C-Angle. The distance from the lowest point of the bladder neck to the pubic bone (PB) and sacrococcygeal joint planes were defined as the BSD. All measurements and analyses of the model were completed by a professional researcher.

2D measurements and analyses

A rectangular coordinate system was built based on the median sagittal image of MRI in the rest state and in maximal Valsalva state respectively. A horizontal line passing through the posterior edge of the PB as the X-axis, and the vertical line for the X-axis through the midpoint of the posterior edge of the PB is the Y-axis. The midpoint and end of the anterior and posterior walls of the urethra and the

vagina, the end of the bladder neck and cervix were marked in the MRI median sagittal images at rest and in the maximal Valsalva state respectively. The Y-value above the X-axis was marked as a positive value, whereas the Y-value below (foot side) was marked as a negative value, and the X-axis on the right side of the Y-axis was marked as a positive value, whereas the left side was marked as a negative value, which measures the position of each marked point (x, y). The total displacement (TD) was measured by the formula $\sqrt{((x_{\text{Valsalva}} - x_{\text{rest}})^2 + (y_{\text{Valsalva}} - y_{\text{rest}})^2)}$.

Statistical analyses

The inter-group mean standard deviation between the SUI group and the control group was tested by Mann–Whitney *U* tests or two independent sample *t* tests to see if there were significant differences between the two population variables. A logistic regression was used to analyze the parameters with statistically significant differences. A receiver operator characteristic (ROC) curve was used to evaluate the accuracy of the continuous variables for detecting and identifying the predictive values of indicators, screening out parameters affecting the occurrence of SUI. The statistical test method was selected according to whether it conforms to the normal distribution. SPSS 26.0 software was used for statistical analysis. $p < 0.05$ was defined as statistically significant.

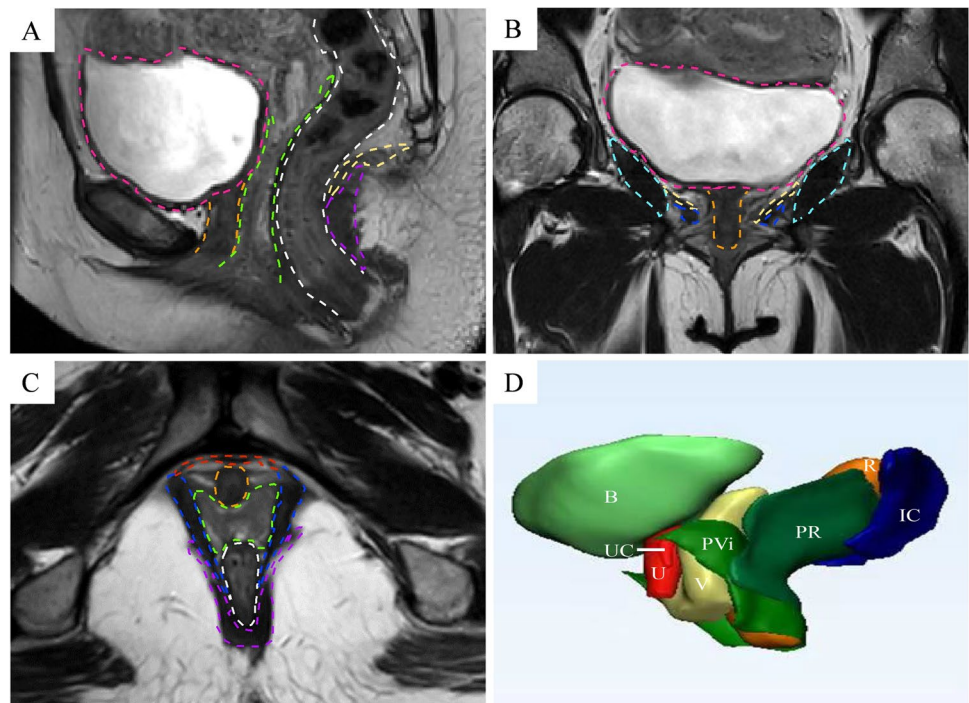
Results

A total of 81 cases were finally included in the study and divided into 40 cases in the SUI group and 41 cases in the normal control group according to the clinical presence or absence of urinary incontinence. There were no statistically significant differences in the mean age, BMI, biparietal diameter, and exam-delivery interval between the two groups ($p > 0.05$).

With the help of Mimics software based on T2-weighted MRI, we reconstructed 3D models of pelvic organs of subjects with and without SUI (Fig. 1), including pelvis, bladder, urethra, vagina, OIM, IC, PR, PVi, and UC. The volume, surface area angle and other parameters of the object were measured using 3-matic (Fig. 2). Then, we used the segmentation function of the software to analyze and measure the relevant components in parts (Fig. 2G–I). The results showed that the BSD, UL, CUV, CUS, CUT, PViV, PRV, and PRS in the SUI group were significantly lower than those in the control group (all, $p < 0.01$), UW, C-Angle, VDW, PViS, PRT, ICV, ICT, and PRV were significantly higher than those in the control group ($p < 0.05$; Table 1).

We marked the points on the MRI during the resting and maximal Valsalva state and measured the spatial positions of each point respectively (Fig. 3), comparing the before

Fig. 1 3D reconstruction of pelvic tissues based on T2-weighted MRI. **A** The sagittal scanning image. **B** The coronal scanning image. **C** The horizontal scanning image. **D** 3D reconstructions of the pubic bone (PB), bladder (B), urethra (U), urethral cavity (UC), vagina (V), rectum (R), iliococcygeus muscle (IC), puborectal muscle (PR), pubovisceral muscle (PVi), urethral compression muscle (CU), and obturator internus muscle (OIM). Red dotted line urethral compression muscle, orange dashed line urethra, green dashed line vagina, white dotted line rectum, deep blue dotted line the pubovisceral muscle, purple dotted line the puborectal muscle, pink dotted line bladder, yellow dotted line the iliococcygeus muscle, wathet dotted line the obturator internus muscle



and after changes in the SUI and control group in the two states. The spatial position of the first site in the Y-direction was significant between the two groups during Valsalva maneuver ($p < 0.01$), and the results of other sites are presented in Table 2. The TDs from rest to maximal Valsalva stage at all sites were significantly greater in the SUI group than in the control group ($p < 0.05$), except for the 3rd site.

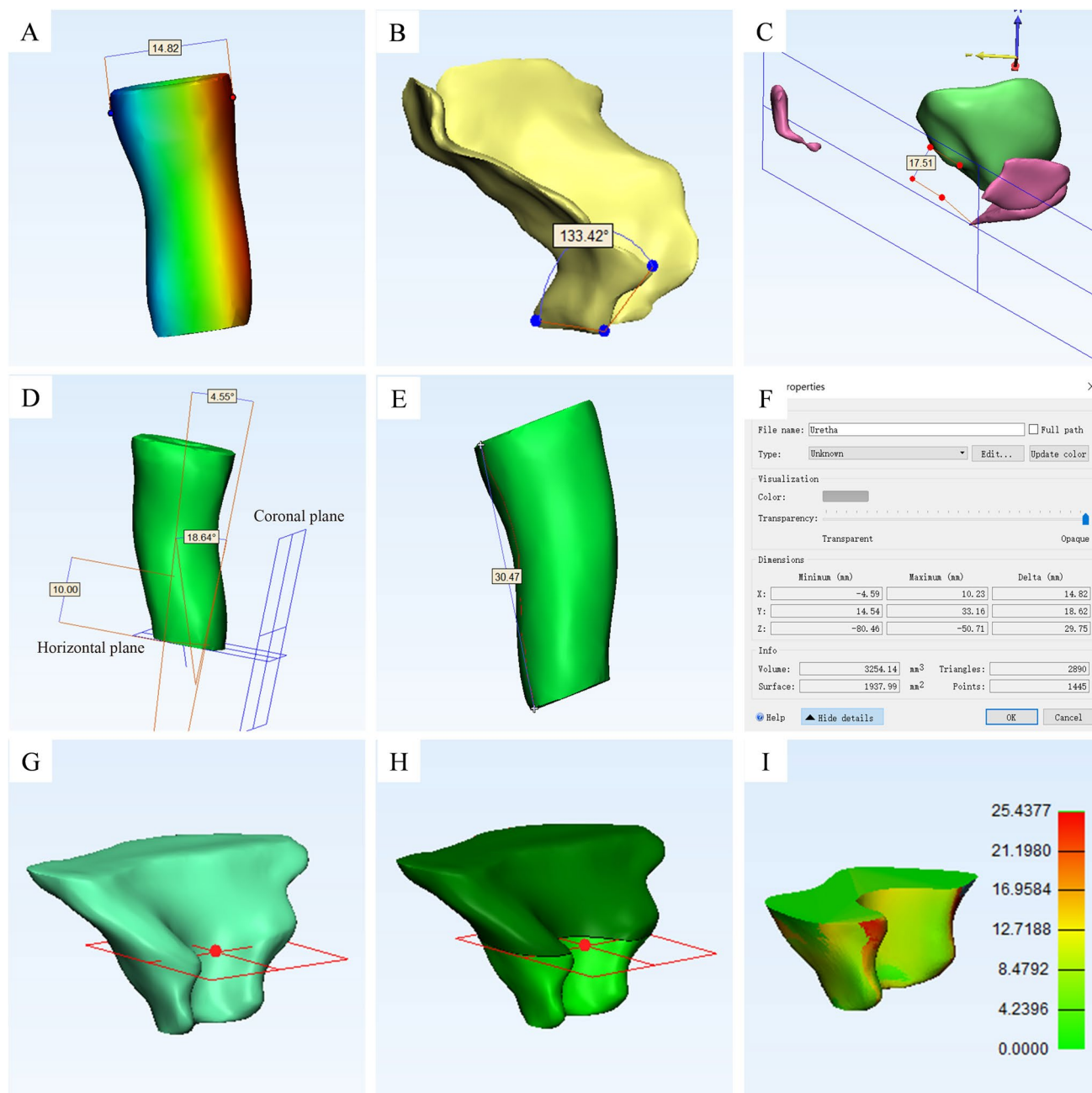
According to the above analysis results, BSD, UL, C-Angle, VDW, CUV, ICV, PViV, PRV, TD of the 1st, 2nd, 4th, 5th, 6th, 7th, and 8th sites were measured as influential factors of SUI. Binary logistic regression analysis showed that the BSD decreased, the CUV decreased, the ICV increased, the TD of the 1st site increased, and the TD of 8th site increased; the parameters correlated significantly with SUI occurrence (Table 3).

The predictive values of relevant parameters for SUI occurrence were analyzed by ROC curve. The results showed that the area under the curve values of BSD, CUV, and ICV were 0.836, 0.800, and 0.717 respectively, indicating that the above parameters were certainly accurate for the diagnosis of SUI. The sensitivities for diagnosing SUI were 72.5%, 87.5%, and 92.5% respectively. The specificities were 85.4%, 61.0%, and 46.3% respectively. The optimal thresholds were 11.455 mm, 0.230 cm³, and 7.745 cm³ respectively (Table 3).

Discussion

Static and dynamic MRI are non-invasive golden imaging techniques for evaluating SUI postpartum [12]. Based on static MRI, this study used a new method combining three planes: horizontal, coronal, and sagittal for 3D reconstruction fusion. These 3D models can be used to measure detailed anatomical parameters of the pelvic floor structures related to SUI. This method does not only avoid the subjective selection of a single plane in 2D measurement, but also compensates for the potential lack of anatomical features in 3D models reconstructed solely using horizontal plane. This study shows that the 3D measurement and the pelvic floor MRI provides more precise and detailed morphological parameters for in-depth exploration of the pathogenesis of SUI.

Previous studies have confirmed that the occurrence of SUI is related to the injury and degeneration of LAM [13]. The LAM is divided into the IC, the PR, and the PVi owing to differences in starting and ending points and course. Sheng et al. showed that urethral closure pressure of women with a PVi tear was 25% lower than those without a PVi tear during an attempted pelvic muscle



contraction by examining the urethral closure pressure of primiparous women [14]. Murad-Regadas et al. used an ultrasound scoring system to assess the correlation between women with vaginal delivery and the severity of symptoms, and found out that patients with a PVi tear had significantly higher incontinence scores [15]. The results of this study indicated that the PViV and PViS of the SUI group were significantly lower than those of the normal group, which was consistent with the studies by Sheng et al. and Murad-Regadas et al. Based on the direct measurement of static MRI, Yasar et al. reported that the average values of the left and right PRT in the urinary incontinence group were

7 mm and 6.23 mm respectively, which were significantly lower than those in the normal group. Consistent with the findings of Yasar et al. [16], we found out that the average value of PRT in the control group was higher than that in the SUI group; the average value of PRT in the SUI group was 6.44 mm.

The difference in the average value of PRT in the above results may be caused by different research objects. The research objects of Yasar et al. [16] include women with symptoms of stress and mixed urinary incontinence, whereas this study focused on primipara with SUI. We then measured the PRV and the PRS indicators, owing to an irregular

Fig. 2 3D analyses of length (mm), width (mm), anteroposterior diameter (mm), volume (cm^3), angle ($^\circ$), distance (mm), thickness (mm), and surface area (cm^2). **A** The leftmost and rightmost points were analyzed by 3-matic software on the X-axis, the urethral width (UW) was measured from the leftmost point to the rightmost point. The UW was 14.82 mm. **B** The anterior point, the last point, and the inflection point of the lower levator ani muscle (LAM) were determined on the Y-axis by 3-matic software. The angle formed by the three points was the inclination angle between the base of the LAM and the lateral wall of the right part (RD-Angle). The RD-Angle was 133.42° . **C** The plane of the posterior margin of the pubic bone and the sacrococcygeal joint was fitted by 3-matic software according to three points, which were used to mark on the 2D plane. The lowest point of the bladder neck fitted by the 2D plane. The distance from the bladder neck to the pubic bone (BSD) is 17.5. **D** The angle between the central line of the proximal and distal urethra and the coronal plane was defined as the A-Angle and the B-Angle respectively. The A-Angle was 4.55° , the B-Angle was 18.64° . The part 10 mm away from the end of the urethra was defined as the distal urethra, and the other part was the proximal urethra. **E** Surface distance from the proximal endpoint of the urethra to the distal endpoint of the urethra was defined as the urethral length (UL). The UL was 30.47 mm. **F** Schematic diagram of the properties of the urethral body. **G** A horizontal plane was identified using 3-matic software according to a point that was used to mark the lowest point of the bladder neck in the 2D plane. **H** The "plane-cutting" tool of the 3-matic software was used to cut the vagina into two parts above and below the bladder neck based on the determined plane. **I** The thickness of the distal region of the vagina (VDT) was analyzed using 3-matic software. The VDT was 25.44 mm. The urethral volume (UV) was 3.12 cm^3 . The urethral surface area (US) was 1.57 cm^2 . VVD distal region of the vagina volume, VSD distal region of the vagina surface area

shape of the PR, it is difficult to calculate the volume and the surface area of PR in 2D measurements, and the calculation based on the elliptical volume formula was not accurate. In this study, PRT and PRV were obtained through 3D automatic analysis, avoiding subjective errors in measurement and improving data accuracy. After analyzing the results using this precise method, we found out that the PRV and PRS in the SUI group were significantly lower than those in the normal group, indicating that the injury of LAM in postpartum women with SUI mainly occurred in the PR and PVi.

Singh et al. suggested that the IC was considered to mainly act on supporting pelvic organs and had little impact on SUI [17]. But our data do not support this perspective, we found out that the average ICS, ICV, and ICT in the SUI group were significantly higher than those in the control group; we speculate that this situation is caused by the potential impact of muscle compensation. Regression analysis showed that the large ICV correlated significantly with SUI and was a risk factor for postpartum SUI.

Mothes et al. found out that normal female urethras were longer than 30 mm and shorter urethras were to be associated with preoperative incontinence symptoms in measuring autologous tissue [18]. Consistent with the measurement results of Mothes et al., we found out that the UL of the SUI group was significantly smaller than that of the

control group, with a mean length difference of 3.5 mm (26.72 ± 3.39 vs 30.18 ± 3.12). The SUI group had a larger UW than the control group in our study. This suggests that women with postpartum SUI have shorter and wider urethras than healthy controls, and UL is an influencing factor for postpartum SUI, but not a risk factor.

According to previous descriptions, our 3D reconstruction fusion technology has been proved not only to be able to restore the morphological characteristics of organs but also to have accurate measurement results [19]. However, our data do not support the findings in some literature that suggested that bladder hypermobility has poor diagnostic efficacy in SUI [20, 21]. Yin et al. [22] indicated that there were no significant differences in the bladder neck mobility between SUI patients and normal women. Despite Mayer et al. examining the bladder neck mobility using a Q-tip test and finding out that it could not provide reliable predictive values for SUI [21], its relative contributions were not evaluated. Differently, this study showed that the BSD and TD of the 1st site in the SUI group were significantly higher than those in the control group, which was consistent with the results of Dietz et al. [23]. We then found out that, compared with the control group, the SUI group had a larger C-Angle. The increase in the C-Angle indicated that the support force provided by the vagina to the bladder neck was weakened, which appeared to increase bladder neck mobility. Logistic regression analysis showed that for every 1-mm increase in the BSD, the relative risk of SUI increases by a factor of 0.478. The BSD had good prediction efficiency for postpartum SUI. Therefore, our study results suggest that the BSD can be used as a diagnostic parameter for postpartum SUI. In this study, the 3D measurements of the BSD and the C-Angle were automatically analyzed using 3-matic software, ensuring accurate and reliable measurement results.

Low urethral closure pressure would lead to the occurrence of SUI [24], and the passive urethral closure pressure was increased owing to the active support provided by urethral compression muscles interacting with hammock structure for urethra and bladder neck, which became the key to maintaining urinary incontinence. We found out that CUV, CUS, and CUT were significantly smaller in the SUI group than in the control group. In addition, controversy exists regarding the relationship between the urethral compression muscle and the external urethral sphincter. Some scholars believed that CUs exist independently [24, 25], whereas others believed that CUs represent only a small muscular protrusion, which is a part belonging to the EUS [26]. We not only observed its presence on imaging, measured and analyzed its volume, surface area versus thickness, but we also found out that the CUV provided a good diagnosis of postpartum SUI, and when the CUV was less than 0.23 cm^3 , the risk of postpartum SUI increased. Despite the differences in nomenclature, there is no doubt that the CU is a critical

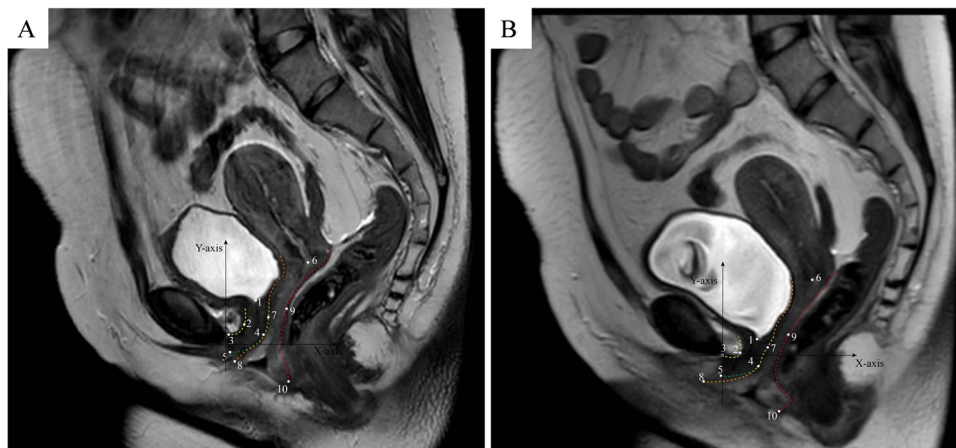


Fig. 3 The marks on static MRI. **A** MRI of the pelvic floor at rest. **B** MRI of the pelvic floor at maximal Valsalva state. *1st site* lowest point of the bladder neck, *2nd site* midpoint of the anterior urethral wall, *3rd site* extremity of the anterior urethral wall, *4th site* midpoint of the posterior urethral wall, *5th site* extremity of the posterior ure-

thral wall; *6th site* extremity of the cervix, *7th site* midpoint of the anterior vaginal wall, *8th site* extremity of the anterior vaginal wall, *9th site* midpoint of the posterior vaginal wall, *10th site* extremity of the posterior vaginal wall

structure for maintaining normal continence. In addition, the causes of stress incontinence in young women are different from the causes in later life, when the deterioration of urethral function takes over as the main causal factor. Therefore, in addition to the support of the structure of the urethra, attention should be paid to the future relationship between the failure of the urethral function itself and postpartum SUI.

The motility of the lower urinary tract is crucial for the assessment of SUI and much attention must be paid to it [11, 27]. Zhao et al. divided the urethra with six equidistant points and found out that the mid-urethra was hyperactive in SUI [11]. Going a step further than Zhao et al., we divided the urethra into anterior and posterior walls separately for segmental study, which contributed to a deeper understanding of the urethral motility status. Different from other sites, only the location of the 3rd site in the X- and Y-directions, as well as TD, showed no statistically significant difference between the two groups, neither at rest nor with Valsalva (Table 2).

Table 2 showed that, compared with the normal group, the SUI group had a larger TD of the 1st, 2nd, and 4th sites ($p < 0.05$), and when pressure was applied, the 1st, 2nd, and 4th site of the SUI group, originally closer to the PB, moved in a more distal direction in the Y-direction compared with the control group (Fig. 4A; $p < 0.05$). Therefore, signs of the larger spatial gap between the 1st, 2nd, and 4th sites, with the formation of a urethral funnel, were observed among primiparous women with SUI. Moreover, the movement characteristics of these sites appear to result in the alteration of the urethra approximately to an anti-“C” shape during the Valsalva maneuver in primipara with SUI compared with healthy primipara.

Our results showed that the TDs of the 2nd and 4th sites in the SUI group were significantly higher than those in the control group, suggesting that postpartum SUI had greater mid-urethral mobility. Although mid-urethral sling is an accepted treatment for SUI, recurrent stress incontinence occurs in 24.2 to 35.7% of women [28, 29]. Relevant research showed that the normal physiological state of the urethra was restored by applying a force to the posterior portion of the bladder neck, improving the surgical success rate [30]. Thus, we believe that the key to the success of the midurethral sling surgery is whether or not the midurethral sling eliminates the deformation of the middle part of the urethra. In addition to limiting the movements of the 1st, 2nd, and 4th sites, which causes the anti-“C” shape of the urethra to disappear, the 5th site is also worth paying attention to. This study showed that the 5th site with a greater TD, originally located lower than the PB, would move in a lower and more ventral direction (Fig. 4A) in the SUI group than in the control group. The difference was statistically significant. Therefore, surgical designs should pay attention to the movement of the posterior end of the urethra after sling surgery is performed to check whether or not it is restricted, in order to ensure the effectiveness of the operation.

At present, there are fewer reports on VDW and vaginal mobility in SUI patients. The anterior vaginal wall is an important part for squeezing the posterior urethral wall during the increase in intra-abdominal pressure [31]. We found out that the VDW of the SUI group was significantly smaller than that of the control group, and that the TDs of the 6th, 7th, and 8th sites were significantly larger in the SUI group than in the control group. Logistic regression analysis showed that every 1-mm increment in

Table 2 Comparison of dynamic MRI measurement parameters between the two groups (mean \pm SD)

| Parameters | SUI | Non-SUI | <i>p</i> |
|--------------------------------|---|--|---------------------|
| 1st site at rest (x, y) | (9.43 \pm 5.35, 23.64 \pm 5.10) | (7.40 \pm 5.27, 24.98 \pm 3.73) | (0.089, 0.183) |
| 1st site with Valsalva (x, y) | (13.29 \pm 5.98, 2.80 \pm 10.39) | (13.63 \pm 6.48, 11.36 \pm 9.50) | (0.705, 0.000*) |
| TD of the 1st site (mm) | 22.61 \pm 9.50 | 16.12 \pm 9.14 | 0.002** |
| 2nd site at rest (x, y) | (4.28 \pm 3.47, 12.83 \pm 3.57) | (3.10 \pm 3.22, 13.57 \pm 3.00) | (0.115, 0.313) |
| 2nd site with Valsalva (x, y) | (13.29 \pm 5.98, 2.80 \pm 10.39) | (13.63 \pm 6.48, 11.37 \pm 9.50) | (0.459, 0.002***) |
| TD of the 2nd site (mm) | 13.10 \pm 4.88 | 10.22 \pm 4.73 | 0.008** |
| 3rd site at rest (x, y) | (1.54 \pm 2.60, 1.79 \pm 3.43) | (1.33 \pm 1.67, 1.91 \pm 3.26) | (0.419, 0.862) |
| 3rd site with Valsalva (x, y) | (-2.55 \pm 4.81, -3.28 \pm 2.96) | (-1.95 \pm 3.44, -2.83 \pm 3.70) | (0.603, 0.554) |
| TD of the 3rd site (mm) | 7.45 \pm 4.10 | 6.61 \pm 3.57 | 0.530 |
| 4th site at rest (x, y) | (16.33 \pm 3.44, 11.45 \pm 5.28) | (14.71 \pm 3.48, 13.68 \pm 3.90) | (0.039*, 0.084) |
| 4th site with Valsalva (x, y) | (13.23 \pm 5.81, -7.39 \pm 6.93) | (14.80 \pm 3.69, -0.02 \pm 8.58) | (0.149, 0.001**) |
| TD of the 4th site (mm) | 19.70 \pm 8.24 | 14.70 \pm 7.70 | 0.006** |
| 5th site at rest (x, y) | (11.13 \pm 3.34, -2.06 \pm 3.92) | (10.77 \pm 3.01, 0.71 \pm 3.78) | (0.615, 0.119) |
| 5th site with Valsalva (x, y) | (1.53 \pm 6.28, -11.18 \pm 4.93) | (4.70 \pm 4.37, -8.95 \pm 6.57) | (0.010*, 0.138) |
| TD of the 5th site (mm) | 14.42 \pm 6.19 | 11.70 \pm 5.07 | 0.033**** |
| 6th site at rest (x, y) | (35.36 \pm 10.01, 49.77 \pm 10.16) | (33.79 \pm 10.92, 49.64 \pm 10.40) | (0.502, 0.954) |
| 6th site with Valsalva (x, y) | (44.82 \pm 12.43, 28.73 \pm 15.68) | (40.20 \pm 12.17, 35.73 \pm 14.65) | (0.119, 0.041****) |
| TD of the 6th site (mm) | 26.13 \pm 14.53 | 18.07 \pm 11.45 | 0.007** |
| 7th site at rest (x, y) | (17.71 \pm 5.05, 18.82 \pm 5.98) | (16.40 \pm 5.49, 19.55 \pm 5.90) | (0.266, 0.584) |
| 7th site with Valsalva (x, y) | (25.24 \pm 7.60, 2.61 \pm 8.91) | (20.85 \pm 6.16, 8.91 \pm 9.07) | (0.005**, 0.002**) |
| TD of the 7th site (mm) | 18.94 \pm 10.04 | 12.96 \pm 7.58 | 0.003** |
| 8th site at rest (x, y) | (3.63 \pm 8.43, -7.01 \pm 4.08) | (2.82 \pm 8.15, -6.55 \pm 4.18) | (0.661, 0.609) |
| 8th site with Valsalva (x, y) | (-3.00 \pm 8.28, -14.40 \pm 6.68) | (0.71 \pm 6.78, -12.90 \pm 5.97) | (0.030*, 0.094) |
| TD of the 8th site (mm) | 13.85 \pm 7.00 | 9.37 \pm 5.59 | 0.007** |
| 9th site at rest (x, y) | (27.97 \pm 7.28, 26.29 \pm 8.65) | (26.76 \pm 7.29, 27.84 \pm 6.50) | (0.457, 0.364) |
| 9th site with Valsalva (x, y) | (35.82 \pm 8.45, 9.32 \pm 11.57) | (31.93 \pm 7.76, 15.32 \pm 11.14) | (0.034*, 0.020****) |
| TD of the 9th site (mm) | 21.14 \pm 11.96 | 15.72 \pm 9.29 | 0.025**** |
| 10th site at rest (x, y) | (25.67 \pm 9.32, -11.92 \pm 7.10) | (26.71 \pm 6.69, -11.00 \pm 5.50) | (0.717, 0.519) |
| 10th site with Valsalva (x, y) | (22.43 \pm 10.38, -19.79 \pm 13.01) | (26.04 \pm 7.92, -17.23 \pm 8.90) | (0.081, 0.043****) |
| TD of the 10th site (mm) | 16.72 \pm 12.02 | 10.92 \pm 5.62 | 0.016**** |

SD standard deviation, TD total displacement, 1st site lowest point of the bladder neck, 2nd site midpoint of the anterior urethral wall, 3rd site extremity of the anterior urethral wall, 4th site midpoint of the posterior urethral wall, 5th site extremity of the posterior urethral wall; 6th site extremity of the cervix, 7th site midpoint of the anterior vaginal wall, 8th site extremity of the anterior vaginal wall, 9th site midpoint of the posterior vaginal wall, 10th site extremity of the posterior vaginal wall

* $p < 0.0001$; ** $p < 0.01$; *** $p < 0.001$; **** $p < 0.05$

TD of the 8th site increased the relative risk of postpartum women suffering from SUI by 1.499 times, indicating that an unstable anterior vaginal wall and slightly narrowed distal vagina could fail to provide effective support to the posterior urethral wall, which leads to the occurrence of SUI. Except for the 10th and 8th sites, the 7th and 9th sites during Valsalva maneuver in the SUI group were all significantly further away from the PB in the horizontal direction, and significantly lower in the vertical direction (Table 2). Based on our findings, we conclude that the postpartum SUI has a narrower VDW, and the middle part of the anterior and posterior walls of the vagina move backward and downward, whereas the distal part moves forward and downward. These results fill the research gaps

in the pattern of vaginal segment activity, which relates to the morphological indicators of the vagina.

In addition, this study has certain limitations. First, our sample size was relatively small, and there were many influencing factors of SUI included in this study; therefore, a larger sample was needed to improve the accuracy of the related factors in logistic regression analysis. Larger samples are needed in the future to confirm and supplement our results. Second, we did not compare the models with the original scan. Third, the axis established by MRI based on horizontal and vertical lines did not take into account the differences in the pelvic inclination in the MRI scanners for our study. However, before static and dynamic MRI examination, all the postpartum women

Table 3 Binary logistic regression and receiver-operating characteristic (ROC) curve analysis

| | Binary logistic regression analysis | | | | ROC curve | | | | |
|-------------------------|-------------------------------------|-------|-------------|---------|-----------|-------|-------------|-------------|----------|
| | β | OR | OR 95%CI | p | Cutoff | AUC | Sensitivity | Specificity | p |
| BSD (mm) | -0.738 | 0.478 | 0.284–0.804 | 0.005* | 11.455 | 0.836 | 0.725 | 0.854 | 0.000*** |
| UL (mm) | -0.679 | 0.057 | 0.229–1.123 | 0.094 | – | – | – | – | – |
| CUV (cm ³) | -19.196 | 0.000 | 0.000–0.012 | 0.011** | 0.230 | 0.800 | 0.875 | 0.610 | 0.000*** |
| ICV (cm ³) | 1.038 | 2.823 | 1.147–6.949 | 0.024** | 7.745 | 0.717 | 0.925 | 0.463 | 0.001* |
| PViV (mm) | -0.747 | 0.474 | 0.195–1.151 | 0.099 | – | – | – | – | – |
| TD of the 1st site (mm) | 0.403 | 1.496 | 1.081–2.072 | 0.015** | 12.924 | 0.682 | 0.850 | 0.439 | 0.005* |
| TD of the 8th site (mm) | 0.405 | 1.499 | 1.108–2.029 | 0.009** | 4.935 | 0.674 | 1.000 | 0.268 | 0.007* |

BSD distance from the bladder neck to the upper edge of pubic bone, UL urethral length, CUV compressor muscle urethra volume, ICV iliococcygeus muscle volume, PViV the pubovisceral muscle volume, TD total displacement, 1st site lowest point of the bladder neck, 8th site extremity of the anterior vaginal wall, AUC area under the curve

* $p < 0.01$; ** $p < 0.05$; *** $p < 0.0001$

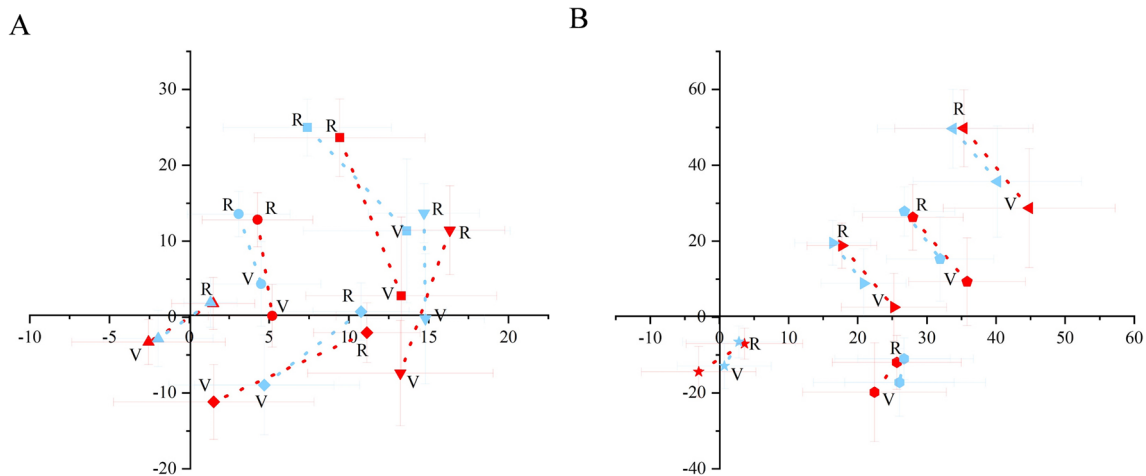


Fig. 4 Displacement trajectories at each site from the resting state to the Valsalva state. **A** Displacement trajectories of the 1st site to the 5th site from the resting state to the Valsalva state. **B** Displacement trajectories of the 6th site to the 10th site from the resting state to the Valsalva state. Red dotted line SUI, blue dotted line non-SUI, square 1st site, circle 2nd site, upper triangle 3rd site, lower triangle 4th site, rhombus 5th site, left triangle 6th site, right triangle 7th site, star 8th site, pentagon 9th site, hexagon 10th site, (0,0) the spatial position

of the posterior edge of the pubic symphysis, R rest state, V Valsalva state, 1st site lowest point of the bladder neck, 2nd site midpoint of the anterior urethral wall, 3rd site extremity of the anterior urethral wall, 4th site midpoint of the posterior urethral wall, 5th site extremity of the posterior urethral wall, 6th site extremity of the cervix, 7th site midpoint of the anterior vaginal wall, 8th site extremity of the anterior vaginal wall, 9th site midpoint of the posterior vaginal wall, 10th site extremity of the posterior vaginal wall

assumed the supine position, with a wedge-shaped cushion placed under the knees, largely maintaining consistency in pelvic position. Finally, although we used a new method of fusion and measurement of 3D models, we restored the anatomical features of the tissue as much as possible. But this approach required building models in three directions (3D), which was an enormous workload. A simpler method of modeling is needed in the future. However, our precise methods provided the possibility of further discovering the variable features of pelvic floor dysfunction diseases.

Conclusions

In conclusion, 3D reconstruction fusion technology based on MRI can accurately measure and analyze morphological changes in pelvic floor structures of postpartum SUI. The BSD, CUV, ICV, bladder neck mobility, and the extremity of the anterior vaginal wall mobility are risk factors for de novo SUI after first vaginal birth, and the BSD, CUV, and ICV have certain value in predicting de novo SUI after first vaginal birth.

Supplementary information The online version contains supplementary material available at <https://doi.org/10.1007/s00192-023-05675-2>

Authors' contributions L. Shi: project development, data collection, manuscript writing; Y. Zhao: data collection, manuscript writing; W. Li: data analysis, manuscript writing; L. Chen: data collection, manuscript writing; W. Shen: data collection, manuscript writing; L. Zhai: administrative support, data collection, manuscript writing.

Funding This study was funded by grants from the National Natural Science Foundation of China (31871212, Lidong Zhai).

Data Availability The data are not publicly available due to their containing information that could compromise the privacy of research participants. This study includes data and imaging from participants. For reasons of reverence, datasets used and/or analysed during the current study are available from the corresponding author on reasonable request.

Declarations

Ethical statement The authors are accountable for all aspects of the work in ensuring that questions related to the accuracy or integrity of any part of the work are appropriately investigated and resolved. The study was conducted in accordance with the Declaration of Helsinki (as revised in 2013). The study was approved by the Institutional Review Board (IRB) of Tianjin first central hospital (registration ID2018NO22KY).

Conflicts of interest None.

References

- Capobianco G, Madonia M, Morelli S, et al. Management of female stress urinary incontinence: a care pathway and update. *Maturitas*. 2018;109:32–8. <https://doi.org/10.1016/j.maturitas.2017.12.008>.
- MacLennan AH, Taylor AW, Wilson DH, Wilson D. The prevalence of pelvic floor disorders and their relationship to gender, age, parity and mode of delivery. *Br J Obstet Gynaecol*. 2000;107(12):1460–70. <https://doi.org/10.1111/j.1471-0528.2000.tb11669.x>.
- DeLancey JO, Miller JM, Kearney R, et al. Vaginal birth and de novo stress incontinence: relative contributions of urethral dysfunction and mobility. *Obstet Gynecol*. 2007;110(2 Pt 1):354–62. <https://doi.org/10.1097/01.Aog.0000270120.60522.55>.
- Li N, Cui C, Cheng Y, et al. Association between magnetic resonance imaging findings of the pelvic floor and de novo stress urinary incontinence after vaginal delivery. *Korean J Radiol*. 2018;19(4):715–23. <https://doi.org/10.3348/kjr.2018.19.4.715>.
- Garriga JC, Isern AP, Carballeira MR, et al. Three-dimensional translabial ultrasound assessment of urethral supports and the urethral sphincter complex in stress urinary incontinence. *Neurourol Urodyn*. 2017;36(7):1839–45. <https://doi.org/10.1002/nau.23193>.
- Peker H, Peker BH. 3D high frequency endovaginal ultrasound evaluation of urethral and pelvic morphology in stress urinary incontinence in first pregnancy. *Eur J Obstet Gynecol Reprod Biol*. 2021;261:148–53. <https://doi.org/10.1016/j.ejogrb.2021.04.037>.
- Feng YK, Wu JH, Zhu H, et al. Three-dimensional measurement and analysis of benign prostatic hyperplasia. *Transl Androl Urol*. 2021;10(6):2384–96. <https://doi.org/10.21037/tau-21-142>.
- Feng YK, Zhang SJ, Zhou Y, et al. Three-dimensional measurement and analysis of morphological parameters of the uterus in infertile women. *Quant Imaging Med Surg*. 2022;12(4):2224–37. <https://doi.org/10.21037/qims-21-812>.
- Shi Q, Wen L, Zhao B, Huang S, Liu D. The association of hiatal dimensions and urethral mobility with stress urinary incontinence. *J Ultrasound Med*. 2022;41(3):671–7. <https://doi.org/10.1002/jum.15748>.
- Shek KL, Dietz HP. The urethral motion profile: a novel method to evaluate urethral support and mobility. *Aust N Z J Obstet Gynaecol*. 2008;48(3):337–42. <https://doi.org/10.1111/j.1479-828X.2008.00877.x>.
- Zhao B, Wen L, Liu D, Huang S. Urethral configuration and mobility during urine leaking described using real-time transperineal ultrasonography. *Ultrasonography*. 2022;41(1):171–6. <https://doi.org/10.14366/ug.21058>.
- Reiner CS, Weishaupt D. Dynamic pelvic floor imaging: MRI techniques and imaging parameters. *Abdom Imaging*. 2013;38(5):903–11. <https://doi.org/10.1007/s00261-012-9857-7>.
- Kim JK, Kim YJ, Choo MS, Cho KS. The urethra and its supporting structures in women with stress urinary incontinence: MR imaging using an endovaginal coil. *Am J Roentgenol*. 2003;180(4):1037–44. <https://doi.org/10.2214/ajr.180.4.1801037>.
- Sheng Y, Liu XF, Low LK, Ashton-Miller JA, Miller JM. Association of pubovisceral muscle tear with functional capacity of urethral closure: evaluating maternal recovery from labor and delivery. *Am J Obstet Gynecol*. 2020;222(6):598.e1–7. <https://doi.org/10.1016/j.ajog.2019.11.1257>.
- Murad-Regadas SM, Fernandes GOD, Regadas FSP, et al. Usefulness of anorectal and endovaginal 3D ultrasound in the evaluation of sphincter and pubovisceral muscle defects using a new scoring system in women with fecal incontinence after vaginal delivery. *Int J Colorectal Dis*. 2017;32(4):499–507. <https://doi.org/10.1007/s00384-016-2750-z>.
- Yasar L, Telci SO, Dogan K, Kaya E, Ekin M. Predictive role of measurement of pelvic floor muscle thickness with static MRI in stress and mixed urinary incontinence. *Int Urogynecol J*. 2019;30(2):271–7. <https://doi.org/10.1007/s00192-018-3663-x>.
- Singh K, Reid WM, Berger LA. Magnetic resonance imaging of normal levator ani anatomy and function. *Obstet Gynecol*. 2002;99(3):433–8. [https://doi.org/10.1016/s0029-7844\(01\)01743-4](https://doi.org/10.1016/s0029-7844(01)01743-4).
- Mothes AR, Mothes HK, Kather A, et al. Inverse correlation between urethral length and continence before and after native tissue pelvic floor reconstruction. *Sci Rep*. 2021;11(1):22011. <https://doi.org/10.1038/s41598-021-01565-z>.
- Feng Y, Wu J, Zhu H, et al. Three-dimensional measurement and analysis of benign prostatic hyperplasia. *Transl Androl Urol*. 2021;10(6):2384–96. <https://doi.org/10.21037/tau-21-142>.
- Hol M, van Bolhuis C, Vierhout ME. Vaginal ultrasound studies of bladder neck mobility. *Br J Obstet Gynaecol*. 1995;102(1):47–53. <https://doi.org/10.1111/j.1471-0528.1995.tb09025.x>.
- Mayer R, Wells TJ, Brink CA, Clark P. Correlations between dynamic urethral profilometry and perivaginal pelvic muscle activity. *Neurourol Urodyn*. 1994;13(3):227–35. [https://doi.org/10.1002/1520-6777\(1994\)13:3<227::aid-nau1930130304>3.0.co;2-a](https://doi.org/10.1002/1520-6777(1994)13:3<227::aid-nau1930130304>3.0.co;2-a).
- Yin YT, Xia ZJ, Feng XY, Luan M, Qin MY. Three-dimensional transperineal ultrasonography for diagnosis of female occult stress urinary incontinence. *Med Sci Monit*. 2019;25:8078–83. <https://doi.org/10.12659/msm.917086>.
- Dietz HP, Clarke B, Herbison P. Bladder neck mobility and urethral closure pressure as predictors of genuine stress incontinence. *Int Urogynecol J Pelvic Floor Dysfunct*. 2002;13(5):289–93. <https://doi.org/10.1007/s001920200063>.

24. Pipitone F, Sadeghi Z, DeLancey JOL. Urethral function and failure: a review of current knowledge of urethral closure mechanisms, how they vary, and how they are affected by life events. *Neurourol Urodyn*. 2021;40(8):1869–79. <https://doi.org/10.1002/nau.24760>.
25. Wang Y, Yao J, Chen N, Liu J, Shi G, Wu Y. Study of female pelvic floor muscle in overactive bladder based on MRI 3D reconstruction. *BMC Urol*. 2022;22(1):132. <https://doi.org/10.1186/s12894-022-01090-9>.
26. Yucel S, Baskin LS. An anatomical description of the male and female urethral sphincter complex. *J Urol*. 2004;171(5):1890–7. <https://doi.org/10.1097/01.ju.0000124106.16505.df>.
27. Zhao BH, Wen LM, Liu D, Huang SY. Visualized urethral mobility profile during urine leakage in supine and standing positions. *Ultraschall Med*. 2023;44(3):e158–63. <https://doi.org/10.1055/a-1700-2862>.
28. Jun T, Yoon HS, Kim HS, Lee JW, Bae J, Lee HW. Recurrence rate of stress urinary incontinence in females with initial cure after transobturator tape procedure at 3-year follow-up. *Investig Clin Urol*. 2017;58(1):54–60. <https://doi.org/10.4111/icu.2017.58.1.54>.
29. Nikolopoulos KI, Betschart C, Doumouchtsis SK. The surgical management of recurrent stress urinary incontinence: a systematic review. *Acta Obstet Gynecol Scand*. 2015;94(6):568–76. <https://doi.org/10.1111/aogs.12625>.
30. Tian D, Gao Z, Zhou H, et al. A comparative study on the clinical efficacy of simple transobturator midurethral sling and posterior pelvic floor reconstruction. *Medicina (Kaunas)*. 2023;59(1):155. <https://doi.org/10.3390/medicina59010155>.
31. DeLancey JO. Structural support of the urethra as it relates to stress urinary incontinence: the hammock hypothesis. *Am J Obstet Gynecol*. 1994;170(6):1713–20. [https://doi.org/10.1016/s0002-9378\(94\)70346-9](https://doi.org/10.1016/s0002-9378(94)70346-9). discussion 1720–3.

Publisher's Note Springer Nature remains neutral with regard to jurisdictional claims in published maps and institutional affiliations.

Springer Nature or its licensor (e.g. a society or other partner) holds exclusive rights to this article under a publishing agreement with the author(s) or other rightsholder(s); author self-archiving of the accepted manuscript version of this article is solely governed by the terms of such publishing agreement and applicable law.